TECHNICAL REPORT ARCCB-TR-94036

EXPERIMENTAL METHODS IN RESIDUAL STRESS MEASUREMENT USING A POSITION-SENSITIVE SINGLE-EXPOSURE SCINTILLATION DETECTION SYSTEM

S.L. LEE
M. DOXBECK
G.P. CAPSIMALIS

DTIC
ELECTE
JAN 13 1995
S G D

SEPTEMBER 1994

DISCLAIMER

The findings in this report are not to be construed as an official Department of the Army position unless so designated by other authorized documents.

The use of trade name(s) and/or manufacturer(s) does not constitute an official indorsement or approval.

DESTRUCTION NOTICE

For classified documents, follow the procedures in DoD 5200.22-M, Industrial Security Manual, Section II-19 or DoD 5200.1-R, Information Security Program Regulation, Chapter IX.

For unclassified, limited documents, destroy by any method that will prevent disclosure of contents or reconstruction of the document.

For unclassified, unlimited documents, destroy when the report is no longer needed. Do not return it to the originator.

REPORT DOCUMENTATION PAGE

Public reporting burden for this collection of information is estimated to average 1 hour per response, including the time for reviewing instructions, searching existing data sources, gathering and maintaining the data needed, and completing and reviewing the collection of information. Send comments regarding this burden estimate or any other aspect of this collection of information, including suggestions for reducing this burden. to Washington Headquarters Services, Directorate for Information Operations and Reports, 1215 Jefferson Davis Highway, Suite 1204, Arlington, VA 22202-4302, and to the Office of Management and Budget, Paperwork Reduction Project (0704-0188), Washington, DC 20503.

1. AGENCY USE ONLY (Leave blank)	2. REPORT DATE September 1994	3. REPORT TYPE AND DATES COVERED Final

4. TITLE AND SUBTITLE
EXPERIMENTAL METHODS IN RESIDUAL STRESS
MEASUREMENT USING A POSITION-SENSITIVE
SINGLE-EXPOSURE SCINTILLATION DETECTION SYSTEM

5. FUNDING NUMBERS
AMCMS: 6111.02.H611.1
PRON: 1A12Z1CANMBJ

6. AUTHOR(S)
S.L. Lee, M. Doxbeck, and G.P. Capsimalis

7. PERFORMING ORGANIZATION NAME(S) AND ADDRESS(ES)
U.S. Army ARDEC
Benét Laboratories, SMCAR-CCB-TL
Watervliet, NY 12189-4050

8. PERFORMING ORGANIZATION REPORT NUMBER
ARCCB-TR-94036

9. SPONSORING / MONITORING AGENCY NAME(S) AND ADDRESS(ES)
U.S. Army ARDEC
Close Combat Armaments Center
Picatinny Arsenal, NJ 07806-5000

10. SPONSORING / MONITORING AGENCY REPORT NUMBER

11. SUPPLEMENTARY NOTES

12a. DISTRIBUTION / AVAILABILITY STATEMENT

Approved for public release; distribution unlimited

12b. DISTRIBUTION CODE

13. ABSTRACT (Maximum 200 words)
In the Denver D-1000-A single-exposure position-sensitive scintillation detection (PSSD) system, surface residual stress measurement in any chosen direction is based on crystalline plane spacings determined in two directions normal to the surface made simultaneously in a single psi tilt. This technical allows fast, noncontacting, and nondestructive biaxial stress analysis. In this report, system performance is characterized by studying the noise, gain, and diffraction peak profiles as a function of diode array element. A four-point bend experiment was performed to determine the elastic constant of the 211 plane of body-centered cubic martensitic steel. Residual stress measurements were performed in several steel specimens and compared to measurements made on a similar system at Pennsylvania State University. Local software development allowed the single-exposure PSSD to run in a multiple-exposure mode for improved accuracy in biaxial stress analysis.

14. SUBJECT TERMS
Residual Stress, Biaxial Stress, X-Ray Diffraction, Position-Sensitive Scintillation Detector, Single-Exposure Technique

15. NUMBER OF PAGES
27

16. PRICE CODE

17. SECURITY CLASSIFICATION OF REPORT	18. SECURITY CLASSIFICATION OF THIS PAGE	19. SECURITY CLASSIFICATION OF ABSTRACT	20. LIMITATION OF ABSTRACT
UNCLASSIFIED	UNCLASSIFIED	UNCLASSIFIED	UL

NSN 7540-01-280-5500

TABLE OF CONTENTS

Tables

List of Illustrations

ACKNOWLEDGEMENTS

INTRODUCTION

Residual stresses, including macro and micro stresses, are caused by the nonuniform plastic flow of previous operations. Most manufacturing processes involving thermomechanical and chemical treatment of components generate residual stresses. In weapon systems, artificial processes are used to induce advantageous residual stress distribution for retarding fatigue crack growth and improving fatigue strength of the component.

In recent years, advances have been made in nondestructive techniques and instrumentation employing x-ray diffraction, ultrasonics, neutron diffraction, and Barkhausen noise techniques for residual stress determination. Among these, x-ray diffraction has been established as one of the most accurate and reliable methods (refs 1-3). The D-1000-A x-ray stress analyzer, manufactured by Denver X-Ray Instruments, is a single-exposure position-sensitive scintillation detection (PSSD) system. It allows fast, noncontacting, nondestructive biaxial surface stress analysis in metals, alloys, and other polycrystalline materials. This report summarizes the experimental methods employed during the calibration of this instrument. Utilizing the four-point bend apparatus with a bar specimen made of ASTM A723 gun steel, x-ray stresses and strain gauge results were compared, and the elastic constant for the 211 plane of martensitic steel was determined. Single-exposure stress analysis was made for several specimens. Local software development has been made to use the single-exposure PSSD for multiple-exposure ($\sin^2\psi$) x-ray diffraction stress analysis.

INSTRUMENTATION

The D-1000-A x-ray stress analyzer is a prototype instrument designed after a Ruud-Barrett PSSD (refs 4,5). The instrument utilizes a miniature x-ray tube that fits inside a cylinder with a 94-mm bore diameter. The operating principles for this detection system, shown in Figure 1, consist of converting incident x-rays into light through cadmium-zinc sulfide scintillation coating; transporting this light to a detector package through fiber optics bundles; amplifying the light intensity through an image intensifier; and converting it into electronic signals through a reticon photodiode array. The PSSD exploits x-ray sources of about 100 to 200 watts and provides a shorter data collection time interval of any x-ray diffraction detection system.

The system currently uses a chromium target tube, whose characteristic radiation does not fluoresce any major alloys in steel. Chromium K-α radiation reflects from the 211 plane of the body-centered-cubic (BCC) martensitic steel at a 2θ angle of 156.41 degrees. The reticon diode arrays, which are solid state scanners, consist of a row of silicon photodiodes, each with an associated storage capacitor upon which the photocurrent is integrated. The device has sensors on 25.4 micron centers with a sensing aperture 430 microns wide. There are 512 diodes in each of the two arrays. The array dimensions are length = 25.4 micron x 512 = 1.3 cm and width = 430 micron or 0.43 mm. The detector, 1.3 cm in length, spans an angle of 21.2 degrees for a focusing circle of radius R_o = 35 mm. To obtain the required sensitivity, the silicon diode array is cooled to approximately -20°C by a copper heat sink connected to a water jacket. The cylinder is hermetically sealed and flushed with nitrogen so that water vapor does not condense on the cooled parts.

An IBM AT computer is connected to the system for data acquisition, control, storage, and analysis. Since the PSSD produces analog signals, data have to go through an analog-to-digital converter and associated electronics. The system software package uses a number of algorithms to correct electronic and mechanical hardware fluctuations, as well as x-ray focusing errors. Specific data fitting algorithms are used for background correction and diffraction peak determination.

1

SINGLE-EXPOSURE X-RAY DIFFRACTION STRESS ANALYSIS

In x-ray diffraction, stress is determined indirectly by the strain it produces. Hooke's law relates stress and strain by the stiffness and compliance moduli. Stress and strain are second rank tensors, while the stiffness and compliance moduli are fourth rank tensors. From symmetry relationships in most crystal structures, the number of independent nonzero constants in these matrices is greatly reduced. Since stress perpendicular to a free surface is zero, our interest focuses on biaxial stress analysis.

Characteristic x-ray radiations scattered from the successive crystalline planes undergo constructive interference if certain geometric conditions satisfying Bragg's law are met. The interplanar lattice d-spacing acts as a strain gauge. Diffraction peak location measurements can be used to determine both residual and loading stresses. As shown in Figure 2, stress is determined from the shift in diffraction peaks located on two opposite sides of the diffraction cone in a single psi tilt:

$$\sigma = \frac{E(S_2 - S_1)}{(1+v) \cdot 4R_o \sin^2\theta \sin(2\beta)} \tag{1}$$

where E is Young's modulus, v is Poisson's ratio, $(S_2 - S_1)$ represents the peak shift between the right and left diffraction peaks, R_o is the radius of the focusing circle, β is the angle the incident x-ray makes with the specimen normal, and θ is the Bragg angle of the unstressed metal (ref 6).

MULTIPLE-EXPOSURE X-RAY DIFFRACTION STRESS ANALYSIS

In single-exposure analysis using PSSD, a single psi tilt gives 12 points on the $\sin^2\psi$ plot. Multiple-exposure x-ray diffraction stress analysis depends on the measurements from multiple psi angles of inclination. Using the PSSD, N number of psi tilts gives 2N number of points on the $\sin^2\psi$ plot for stress determination by the least squares fit of a line. Multiple-exposure stress analysis using PSSD has advantages over both the single-exposure technique using PSSD and the conventional multiple-exposure technique using a single detector. Local software development has been made to use the PSSD for multiple-exposure biaxial stress analysis.

EXPERIMENTAL METHODS

Surface Preparation

X-ray penetration depends on the x-ray wavelength and the absorption coefficient of the specimen. For chromium x-rays on steel samples, penetration is about twenty microns. To make an accurate residual stress determination, removal of the specimen surface affected by cold working, e.g., grinding and polishing, corrosion, oxidation, and grease and polymer coatings, is necessary. This is done by machine and hand polishing, metallographic polishing, and then electropolishing of the specimen surface. We experimented with current density settings, concentrations of the polishing bath, and used both lead and stainless steel mesh as the cathode in the electropolishing procedure. Figure 3 shows the electropolishing setup used in our experiments.

Detector Gain

When a constant x-ray flux is incident on the detector, pixel-to-pixel differences in total detection efficiency give rise to gain variations. The variations in the scintillation coating thickness, scintillation conversion efficiency, variable amplification of the image intensifier, nonuniform sensitivities of the silicon diode, fiber optics variations, and coupling factors can contribute to the nonuniformity of the gain signals.

To make pixel-to-pixel efficiency correction, gain signals were obtained by irradiating a glass surface with the x-ray beam at the same geometry the stress measurements were to be made. Since glass is an amorphous solid, it should have a uniform diffraction intensity distribution versus angle 2θ in the far back reflection range.

To investigate the uniformity and stability of the gain signal, a log of gain signal intensity versus diode array element was plotted at various integration times as shown in Figure 4 and at various tube currents as shown in Figure 5. Large pixel-to-pixel intensity variations were observed, especially in the right detector. As shown in the following sections of this report, diffraction profiles have to be corrected for nonuniform gain variations. Figure 6 shows that electronic drift in the detectors causes a gain shift. Two traces of gain signals versus diode array elements were recorded at subsequent times using the same integration time, tube current, and voltage, and they were plotted on the same graph. Figure 7 shows the effect of the noisy gain on the noise- and gain-corrected diffraction profiles. Gain stability and statistics are essential in accurate peak location determination. In this work, gain signals were obtained in 5- to 10-second integration times. It was continuously and carefully monitored for possible electronic gain drift.

Detector Noise

Possible light leaks and the electronic dark current both in the image intensifier and diode arrays contribute to the detector noise, which is detected when no x-rays are applied. The dark current in the diode's arrays increases with the temperature of the arrays. Detector noise signals were collected for both the left and right detectors in the PSSD and were used to correct for the gain and profile readings.

Figure 8 is a plot of the average noise variation with detector integration time for the left and right detectors in the PSSD. This plot indicates that the right detector has a noise offset of 87, and the left detector has a noise offset of 25. To equalize the noise offsets, potentiometers within the instrument have to be adjusted. At an integration time near forty seconds, the curve begins to show an exponential behavior. At an integration time less than ten seconds, which was used throughout this work, a linear relationship between noise and the integration time is observed. A formula was derived from this plot and system software was modified to normalize integration time differences for the noise, gain, and profile

$$Noise(t_2) = Noise(t_1) + (t_2 - t_1) \cdot Slope \qquad (2)$$

where t_1 and t_2 are two different integration times.

Diffraction Profile

The intensity of the diffraction profile is proportional to the intensity of the characteristic radiation, which is in turn linearly dependent on the tube current and nonlinearly on the tube high voltage. In this work, a tube voltage of 80 kilovolts and a current of 6 milliamps were used. Integration time for the diffraction profiles ranged between 2 and 10 seconds. Enough sampling time should be allowed without saturating the charge capacitor.

3

Diffraction peak profiles are noise-corrected and divided by the gain efficiency to normalize the pixel-to-pixel gain sensitivities. System software was modified to perform this operation.

$$P(i) = (Profile(i) - Noise(i))/(Gain(i) - Noise(i))$$ (3)

To obtain accurate stress measurement, sufficient integration time should be allowed for the profile and the gain signal. Diffraction peak profile determination was found to be difficult for noisy gain.

Specimen Displacement Error

If the irradiated diffraction volume is displaced from the center of the diffractometer, there is a relative peak shift between psi = 0 and psi = ψ due to specimen displacement error. The Denver x-ray stress analyzer has a Ω-goniometer geometry, and the error in 2θ location is given by Eq. (4):

$$\delta(\Delta 2\theta) = (\Delta 2\theta)_{\psi=0} - (\Delta 2\theta)_{\psi=\psi} = \left(\frac{360}{\pi}\right)(\Delta X)\cdot\cos\theta\left[\frac{1}{R_o} - \frac{\sin\theta}{R\sin(\theta+\psi)}\right]$$ (4)

where

$$R = R_o \frac{\cos(\psi+(90°-\theta))}{\cos(\psi-(90°-\theta))}$$

In Eq. (4), R_o is the diffractometer radius, ΔX is the specimen displacement error, θ is Bragg's angle, and ψ is the psi tilt. When the specimen is too high, ΔX is positive. When the specimen is too low, ΔX is negative. In the $\sin^2\psi$ plot, high specimen position contributes to negative slope and compressive stress state. Low specimen position contributes to positive slope or tensile stress state. Precision specimen alignment by a micrometer dial-gauge indicator or laser-sensor indicator is suggested. ASTM recommends zero stress standard of loose powered iron. In this work, stress-free 400 mesh iron powder was used to obtain zero stress correction and to check for specimen alignment. Diffraction peak profiles for zero stress powder are given in Figures 9 and 10.

Peak Location Determination

Before the diffraction peaks can be located, the raw diffraction peak intensity profiles must be processed by several correction algorithms as provided by the PSSD system software (ref 7):

1.   Incoherent bremsstrahlung background radiation subtraction.

2.   Lorentz polarization absorption intensity corrections.

3.   Planer instead of curved fiber optics surfaces were used. To correct for the fiber optics alignment in the location of the center of the x-ray sensitive fiber optics, a semi-empirical parabolic regression method was used.

4.   Iterative correction for the uncertainty in the detector circle to specimen distance R_o.

4

Li and Sun (ref 8) studied contributions to the background radiation in x-ray stress analysis following derivations from diffraction physics. They proposed a nonlinear equation for background correction dependent on 2θ and the psi tilt, which agreed well with the experimental background curve. Furthermore, we propose that the cross correlation technique be used to determine the diffraction peak shift for weak and noisy diffraction profiles that might occur in certain crystalline structures. In this work, a straight line background fitting algorithm was used. The user determines a range for the starting and ending pixel locations to make the background correction. The user can select the percentage of the upper peak intensity profile in the analysis for the parabolic fit. We found that 70 to 80 percent of the maximum peak intensity is good for the parabolic peak determination.

Cross Correlation Technique

The cross correlation technique can be applied to determine diffraction peak shift, especially for weak and noisy diffraction profiles that might occur in certain crystalline structures. By cross correlating diffraction peak intensity versus diode array element signal at psi = 0 with signals at psi = ψ_1 and psi = ψ_2, respectively, residual stress can be calculated from the diffraction peak shift. An alternate method is to cross correlate the left detector signal (I^{ψ}_1) and the right detector signal (I^{ψ}_2). The cross correlation function for each ψ tilt is given by

$$F_j^{\psi} = \sum_{i=1}^{512} I_i^{\psi_1} + I_{i-j}^{\psi_2}$$ (5)

where i,j are diode array element indices. From the location of the maximum in the cross correlation function, peak shift $(S_2 - S_1)$ in Eq. (1) can be obtained.

FOUR-POINT BEND CALIBRATION AND ELASTIC CONSTANT DETERMINATION

A four-point bend instrument was used to compare the x-ray and strain gauge stress measurements. A strain gauge was attached to a 6 by 1 inch ferritic steel specimen made from ASTM A723 gun steel, and both tensile and compressive stresses were applied. In Figures 11 and 12, the raw and corrected peak profiles for the ferritic steel specimen are shown for the right and left detectors, respectively. In Figure 13, the x-ray stress is plotted versus strain gauge stress. The elastic stress constant was determined from the slope of the curve as follows:

$$\sigma = \left(\frac{E_{hkl}}{1+v}\right)(S_2 - S_1)\left(\frac{0.0254}{4R_o \sin^2\theta \sin(2\beta)}\right)$$

$$\frac{E_{hkl}}{1+v} = \left(\frac{\sigma}{S_2 - S_1}\right)\left(\frac{1}{K}\right) \text{ where } K = \frac{0.0254}{4R_o \sin^2\theta \sin(2\beta)}$$ (6)

Our experiment indicated that the constant $E_{hkl}/(1+v) = 23.9 \cdot 10^6$ psi. The quantity was determined to be $23.5 \cdot 10^6$ psi for the same specimen using the stress analyzer at the Materials Research Laboratory, Pennsylvania State University during our visit.

STRESS ANALYSIS OF M106 SHELL SAMPLE

In Figure 14, the raw and corrected right detector peak profiles for the inside surface axial stress of an M106 shell section are shown. The left detector inside surface hoop stress profiles of an M106 shell section are shown in Figure 15. In Figure 16, the multiple-exposure technique was used for the M106 shell inside axial stress determination. Psi tilts at 12, 20, 25, and 30 degrees give pairs of data points (1,5), (2,6), (3,7), and (4,8) on the graph. D is the interplanar spacing of the planes at nonzero psi and D_o is the interplanar spacing of an unstressed metal. The D_o value was obtained from the literature (ref 9). Linear regression analysis was used to obtain the slope for residual stress determination. In Table 1, the stress results measured at Benét Laboratories are given along with measurements from Pennsylvania State University. Errors quoted represent data dispersion in successive measurements, including statistical error, systematic error, and error due to goodness of fit in the multiple-exposure analysis. Residual stress accuracies are expected to be approximately ± 10 Ksi. The measurements are in good agreement--Benét's values were slightly higher than Pennsylvania State's.

Table 1. Residual Stresses in a Shell Specimen

Stress Orientation	Benét Labs*	Penn State**	Benét Labs***
	Stress (Ksi)	Stress (Ksi)	Stress (Ksi)
inside hoop	-42.1 ± 3.3	-39.1 ± 3.1	-43.5 ± 2.6
inside axial	-43.4 ± 3.3	34.6 ± 1.8	-40.3 ± 3.9
outside hoop	-39.9 ± 1.4	-35.0 ± 1.6	-46.3 ± 3.2
outside axial	-39.1 ± 3.2	-35.3 ± 1.7	-43.4 ± 2.6

*Denver D-1000-A Single-Exposure Stress Analyzer (local software modification)
**Pennsylvania State University Single-Exposure Stress Analyzer
***Denver D-1000-A Multiple-Exposure Measurements (local software development)

CONCLUSION

Experimental methods using Denver D-1000-A single-exposure position-sensitive scintillation detection system (PSSD) are given in this report. Characteristics of noise, gain, and diffraction profiles were studied as a function of system parameters such as integration time, number of iterations, and x-ray tube current and voltage. A four-point bend experiment was performed for an ASTM A723 steel specimen. Elastic constant of the 211 plane of BCC steel was determined. Local software development was made to allow the single-exposure PSSD to run in a multiple-exposure mode. The technique improves accuracy in the $\sin^2\psi$ biaxial stress analysis using the PSSD. Residual stress analyses were made for several ordnance steel specimens.

Suggested software enhancements include cross correlation technique for peak shift determination; capability to determine peak position by profile fit to Gaussian, Lorentzian, and Pearson VII profile types; layer removal stress corrections; and triaxial stress analysis for complete stress tensor determination.

Suggested system hardware improvements include: (1) uniform and stable gain by recoating the scintillation detector; (2) stable current and voltage power supply and associated electronics; (3) precision specimen alignment by micrometer dial-gauge or laser-sensor indicators; (4) automated psi motion control for multiple-exposure stress analysis; and (5) automated radiation shutter. By the application of an extended or mobile photodiode array and x-ray tubes of other wavelengths, Denver D-1000-A PSSD can be expanded to study other metals, alloys, and composite materials.

REFERENCES

1. M.E. Hilley, "Residual Stress Measurement by X-Ray Diffraction," *SAE J784a*, SAE Information Report, Society of Automotive Engineers, Inc., 1980.

2. B.D. Cullity, *Elements of X-Ray Diffraction*, 2nd Edition, Addison-Wesley Publishing Company, Reading, MA, 1978.

3. I.C. Noyan and J.B. Cohen, *Residual Stress, Measurement by Diffraction and Interpretation*, Springer-Verlag, New York, 1987.

4. C.O. Ruud, "Position-Sensitive Detector Improves X-Ray Powder Diffraction," *Industrial Research and Development*, January 1983, pp. 84-87.

5. C.O. Ruud, "X-Ray Analysis and Advances in Portable Field Instrumentation," *Journal of Metals*, Vol. 31, No. 6, June 1979, pp. 10-15.

6. J.T. Norton, "X-Ray Stress Measurement by the Single-Exposure Technique," *Advances in X-Ray Analysis*, Vol. 11, Plenum Press, NY, 1968, pp. 401-410.

7. *D-1000-A Stress Analyzer Instruction Manual*, Denver X-Ray Instruments, Inc., Version 2.0, May 1987.

8. J. Li and Y. Sun, "Background Analysis and Its Correction for X-Ray Stress Measurements," in: *Residual Stresses in Science and Technology*, (E. Macherauch and V. Hauk, eds.), International Conference on Residual Stresses, Vol. 1, 1987.

9. I.C. Noyan, "Determination of the Unstressed Lattice Parameter for Triaxial Residual Stress Determination by X-Rays," Office of Naval Research, Technical Report No. 14, July 1984.

LIQUID COOLED HEAT SINK

THERMOELECTRIC COOLER

COOLING CONDUCTION BLOCK

ELECTRONIC CIRCUITRY

SOLID STATE SCANNERS

MASK WITH FIBER OPTIC COUPLERS

PROXIMITY FOCUSED IMAGE INTENSIFIER

SCINTILLATION COATING

METALLIZED MYLAR

FIBER OPTIC BUNDLE
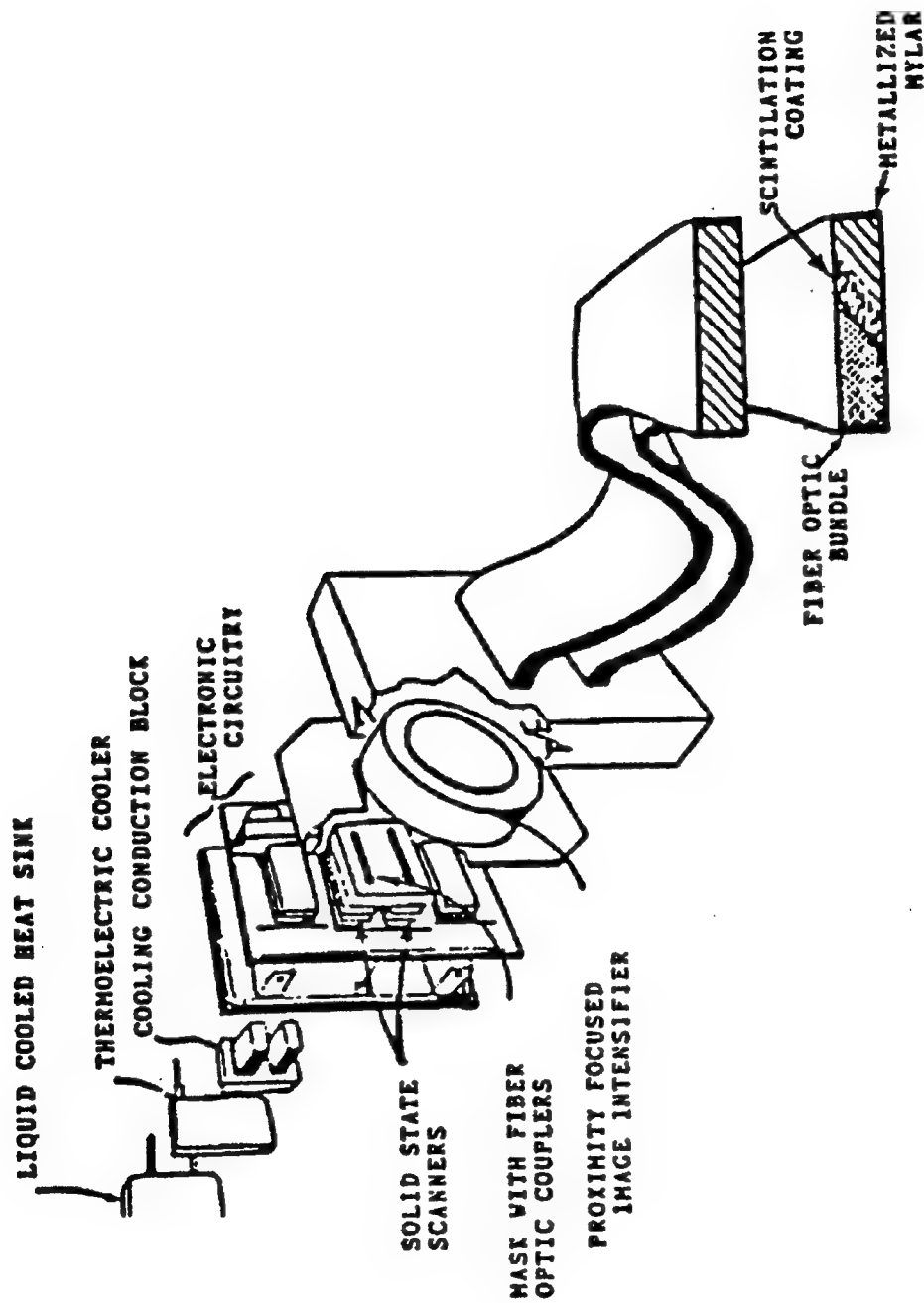
Figure 1. Schematic of the D-1000-A position sensitive scintillation detection system.

9

Figure 2. Single exposure PSSD residual stress determination.
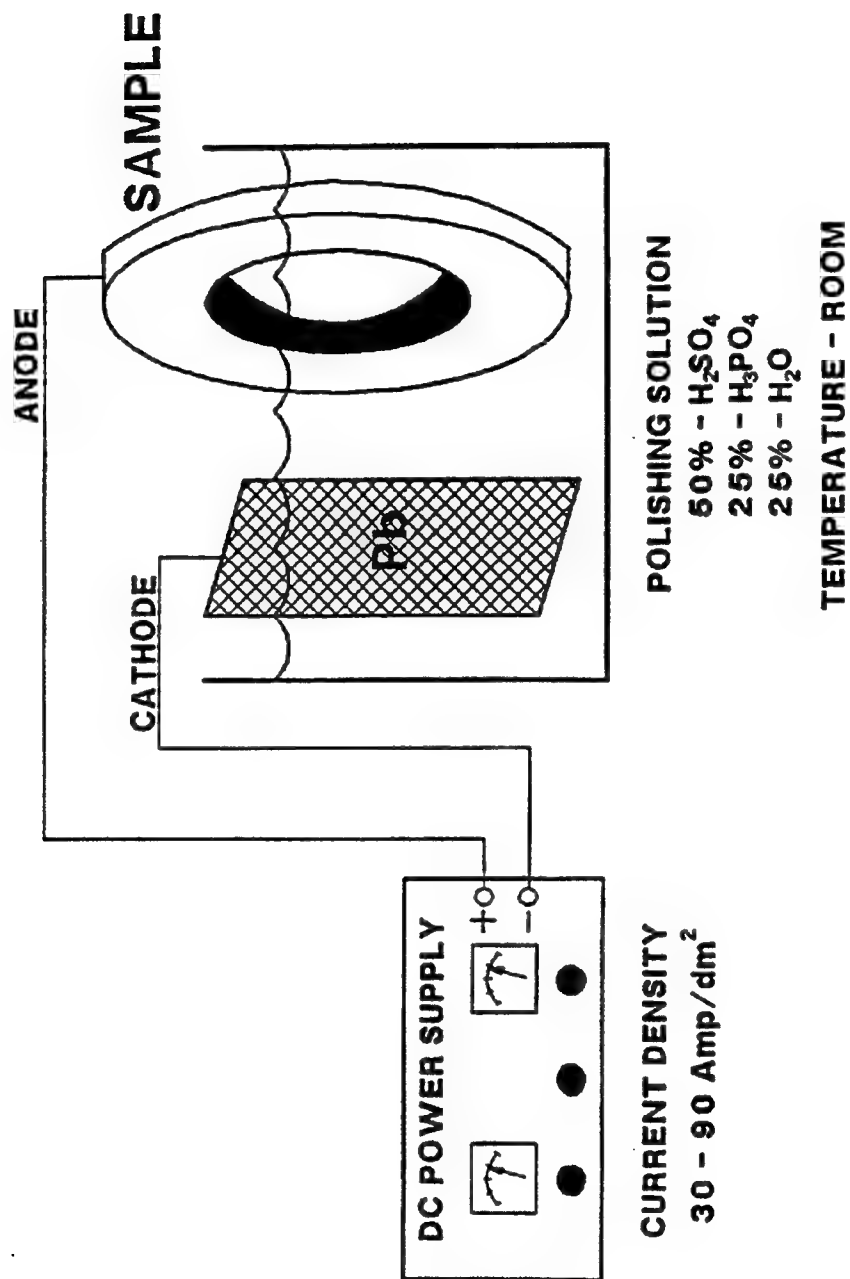
Figure 3. Drawing of electropolishing apparatus.
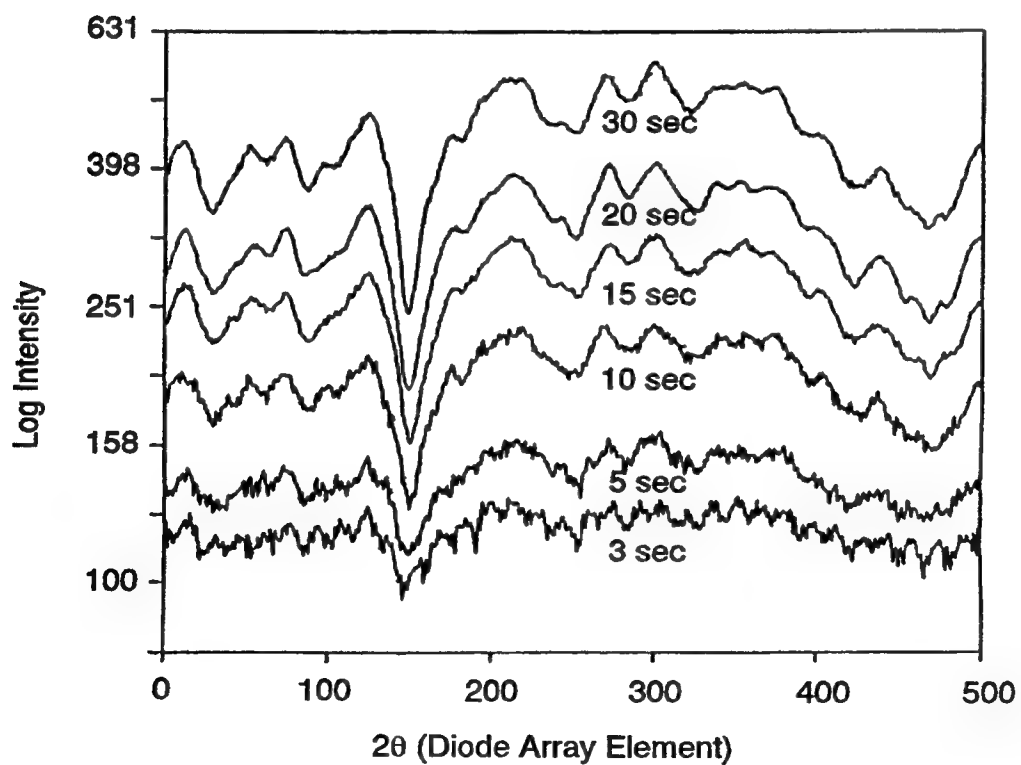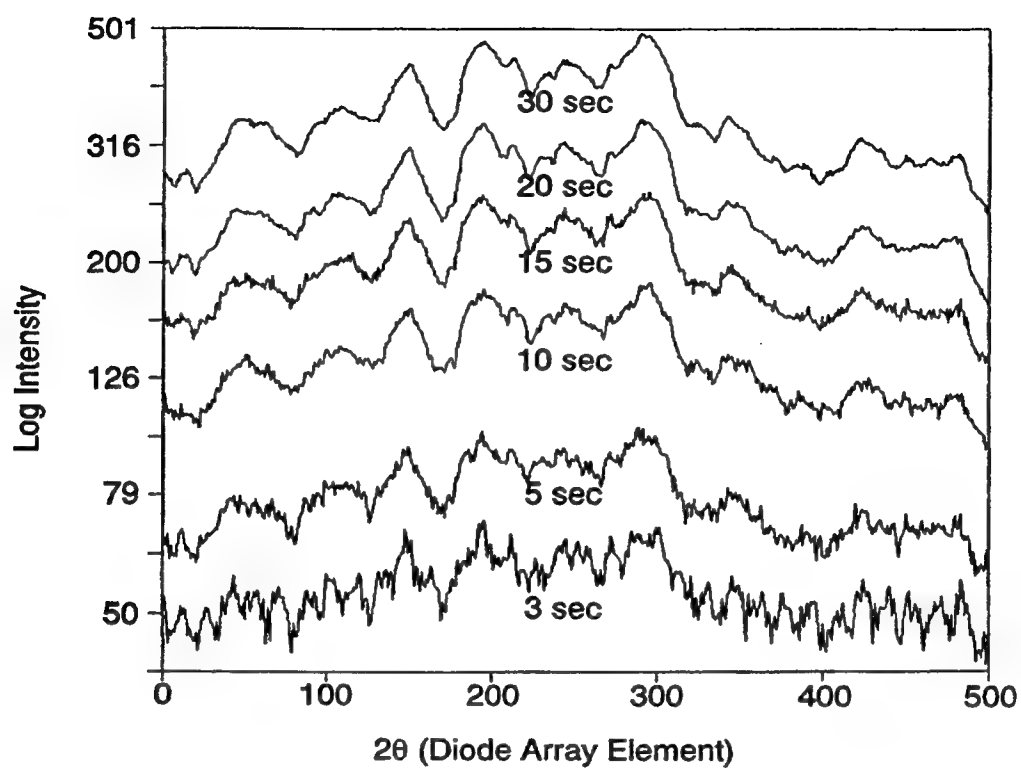
Figure 4. Left & right detector gain for various integration times.
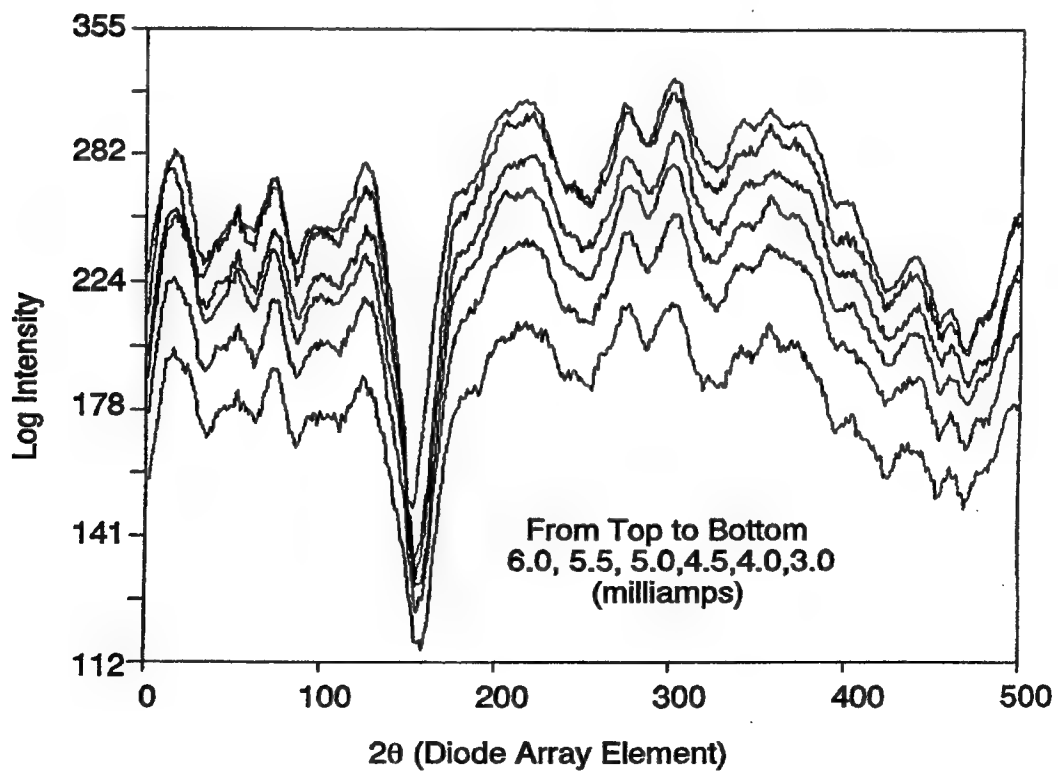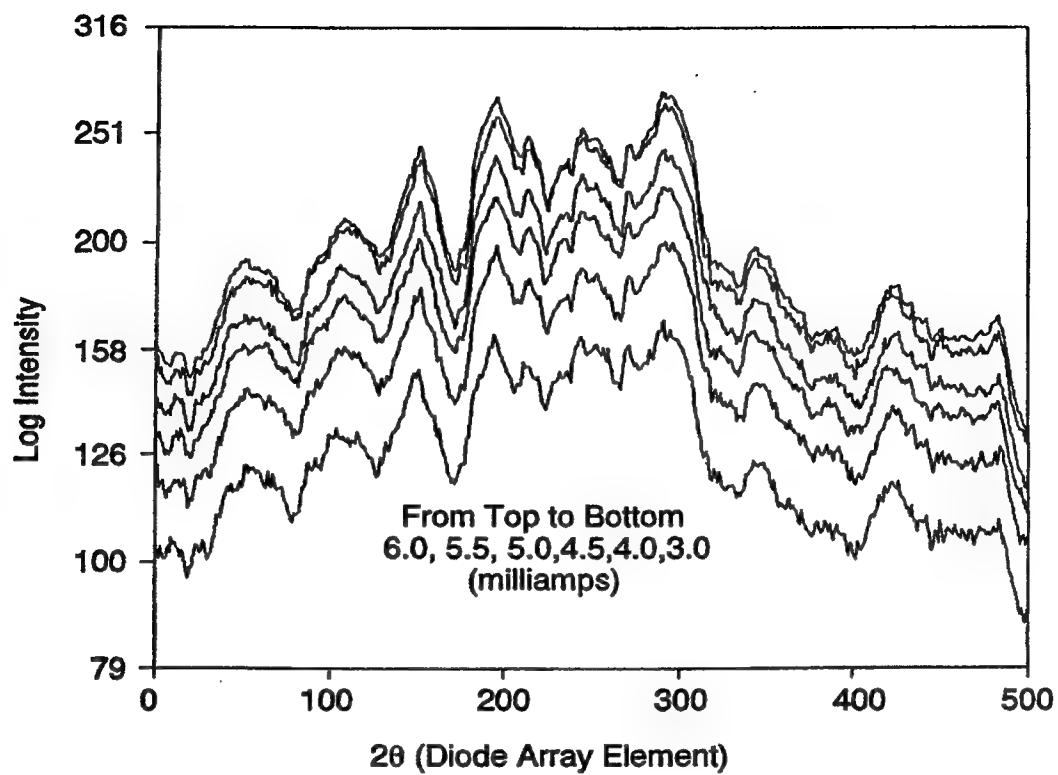
Figure 5. Left & right detector gain for various tube currents.
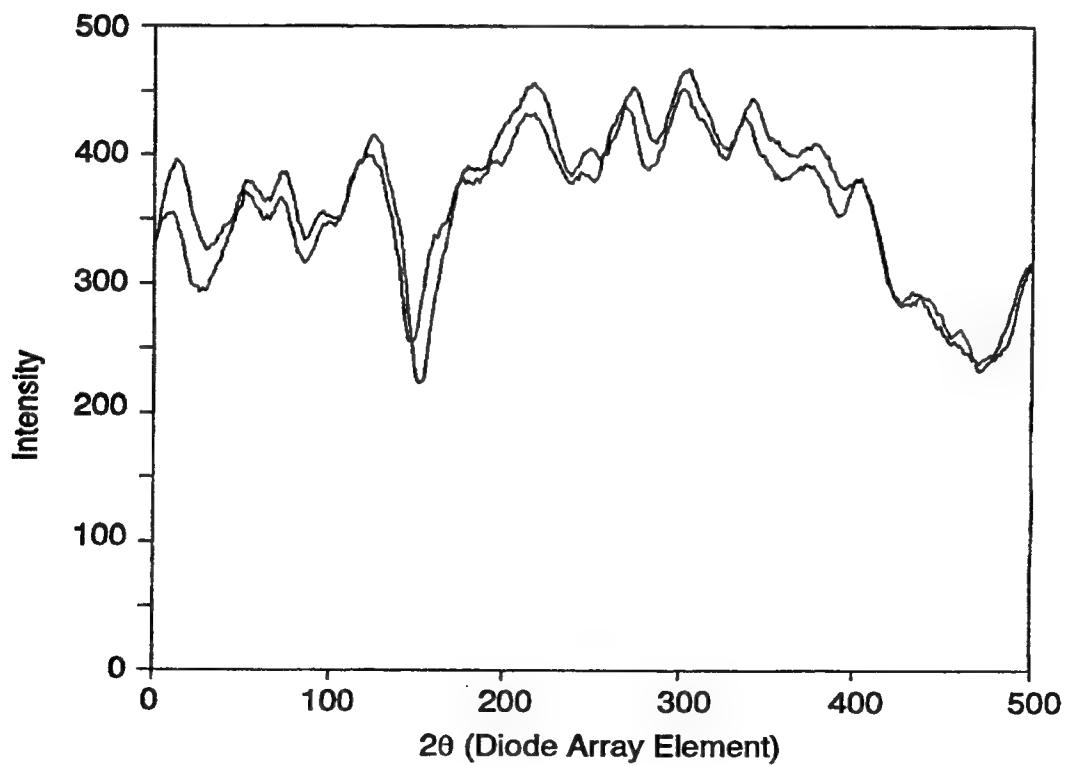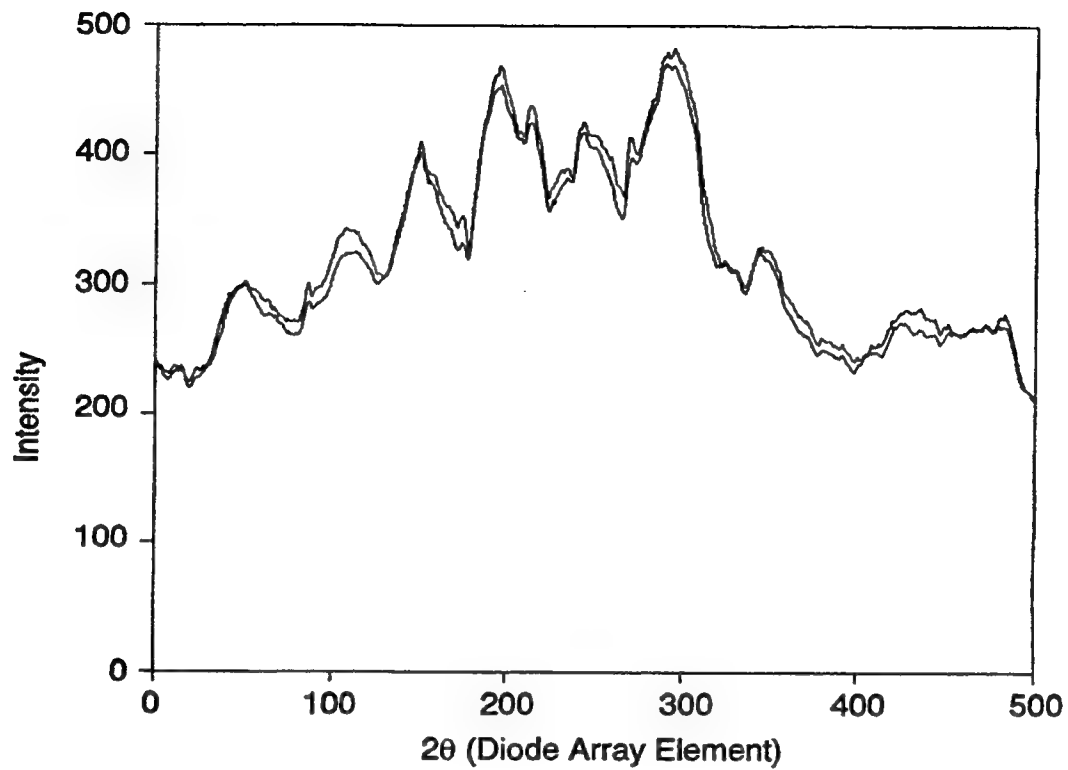
Figure 6. Left & right detector gain signals indicating shift in peak locations due to electronic drift.
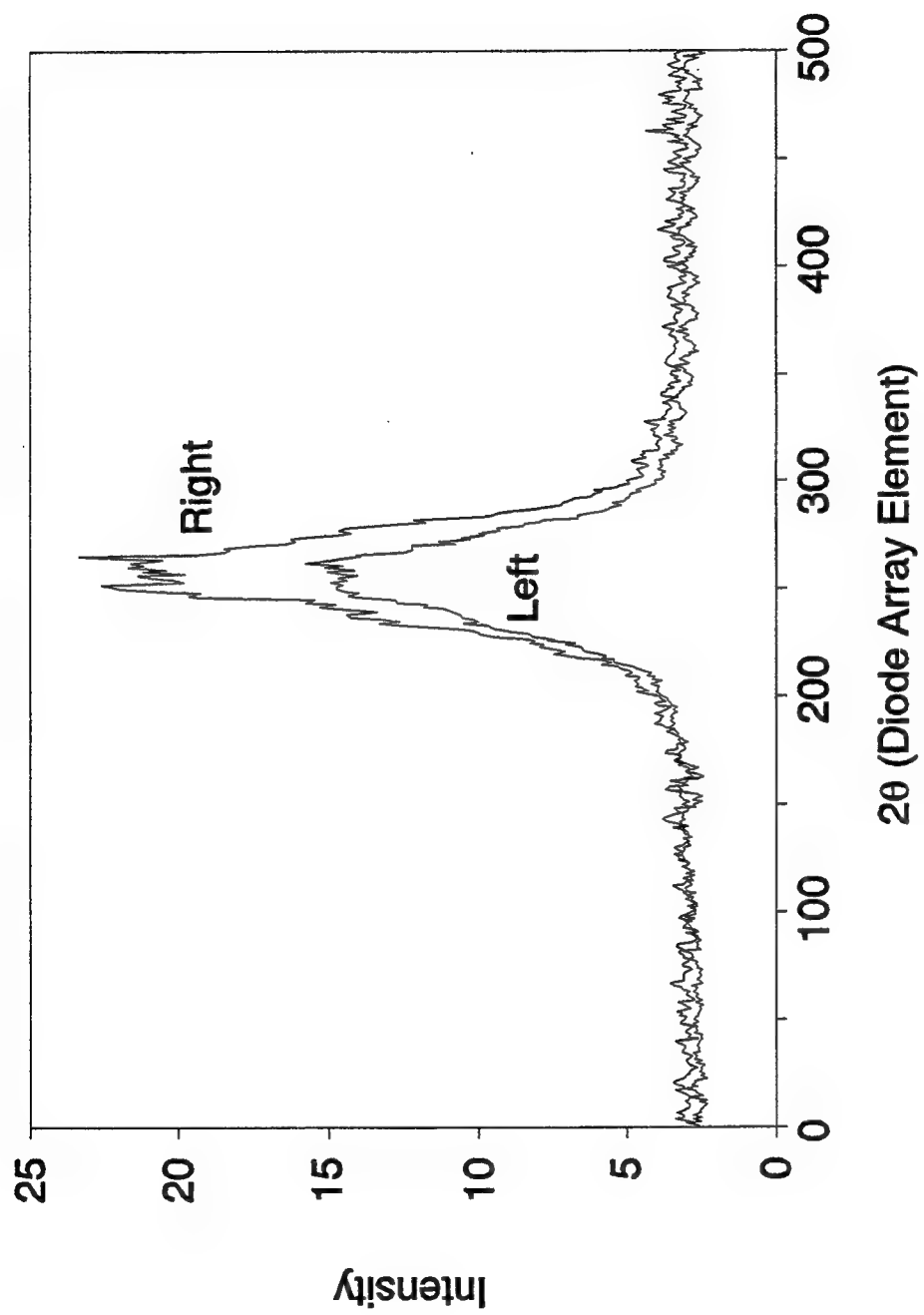
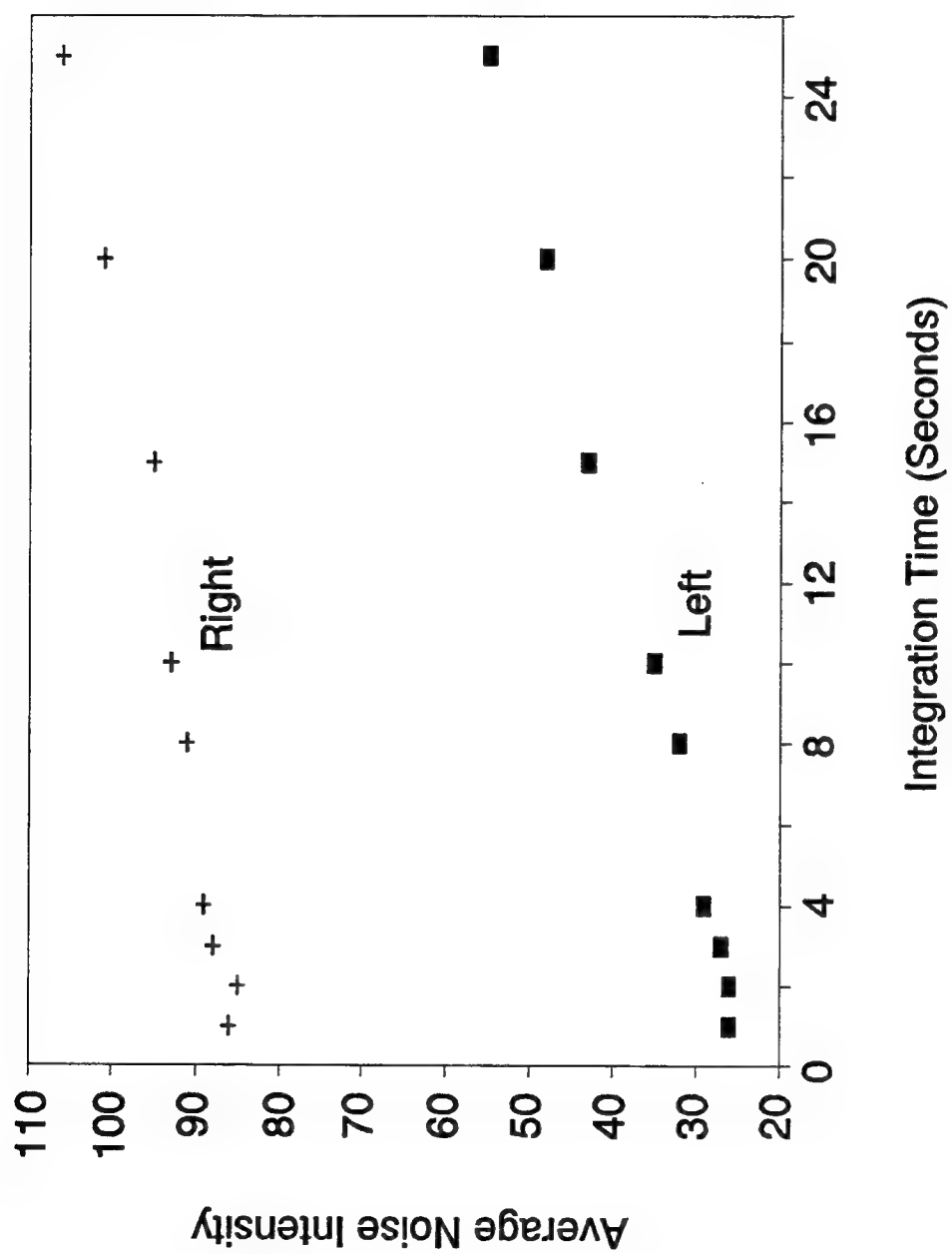Figure 7. Effect of noisy gain on noise- and gain-corrected diffraction profiles.

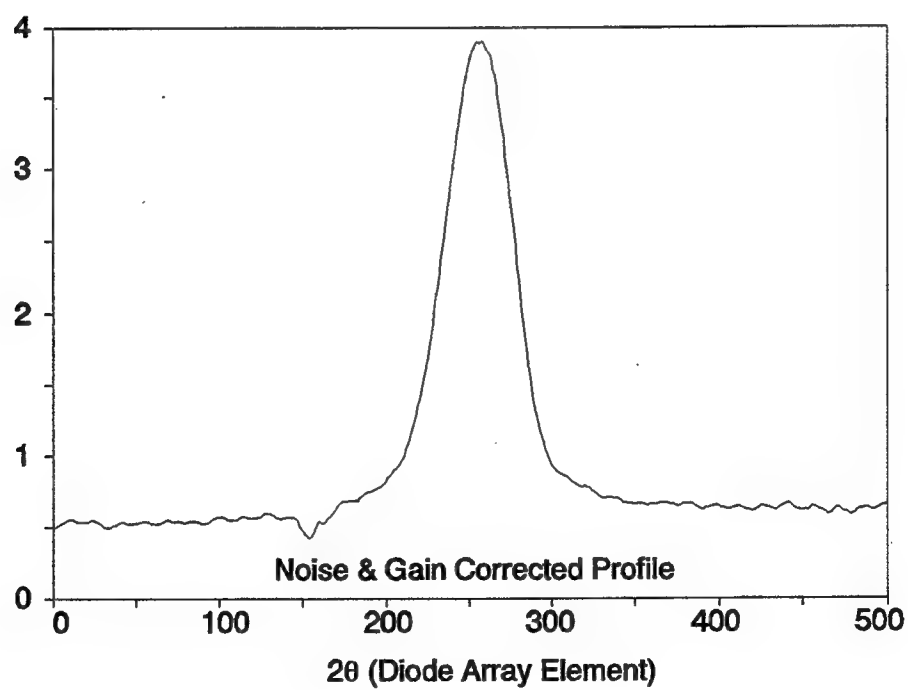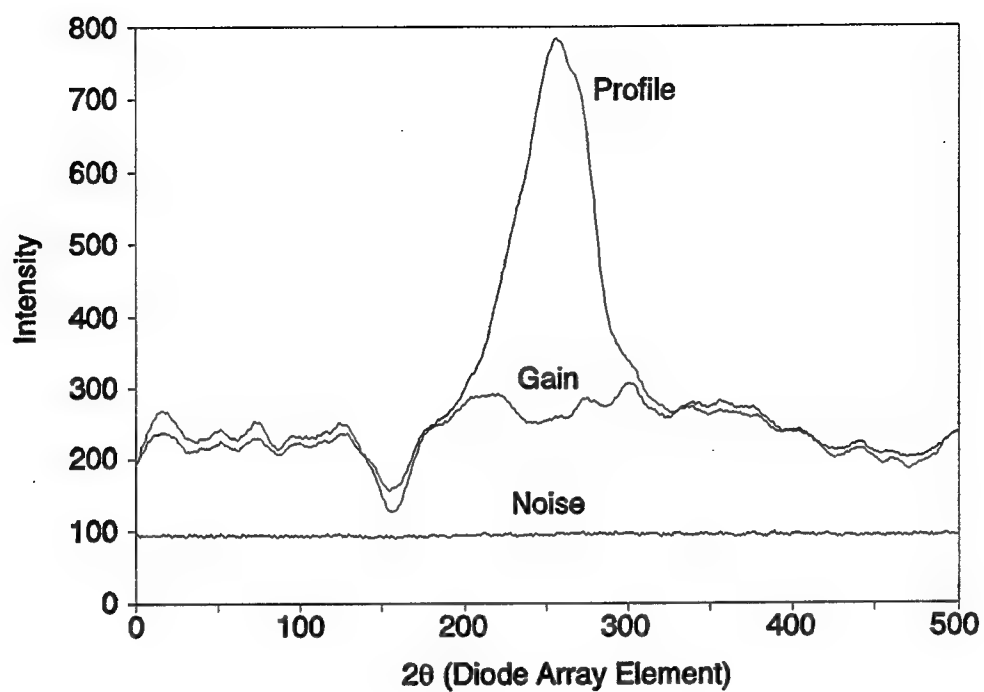Figure 8. Average left and right detector noise versus integration time.

Figure 9. Right detector diffraction profiles for zero stress 400 mesh iron powder.
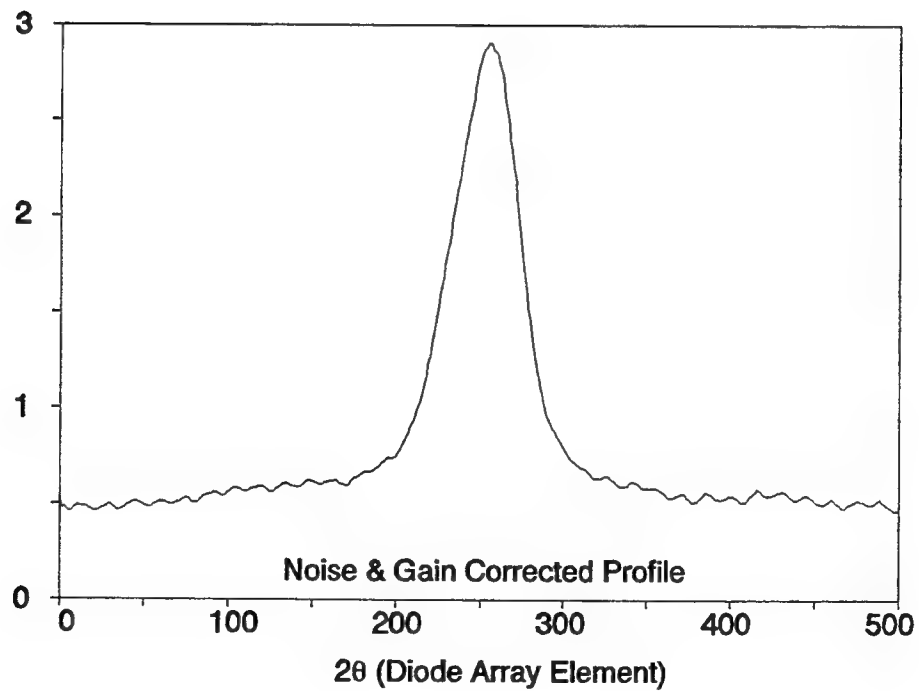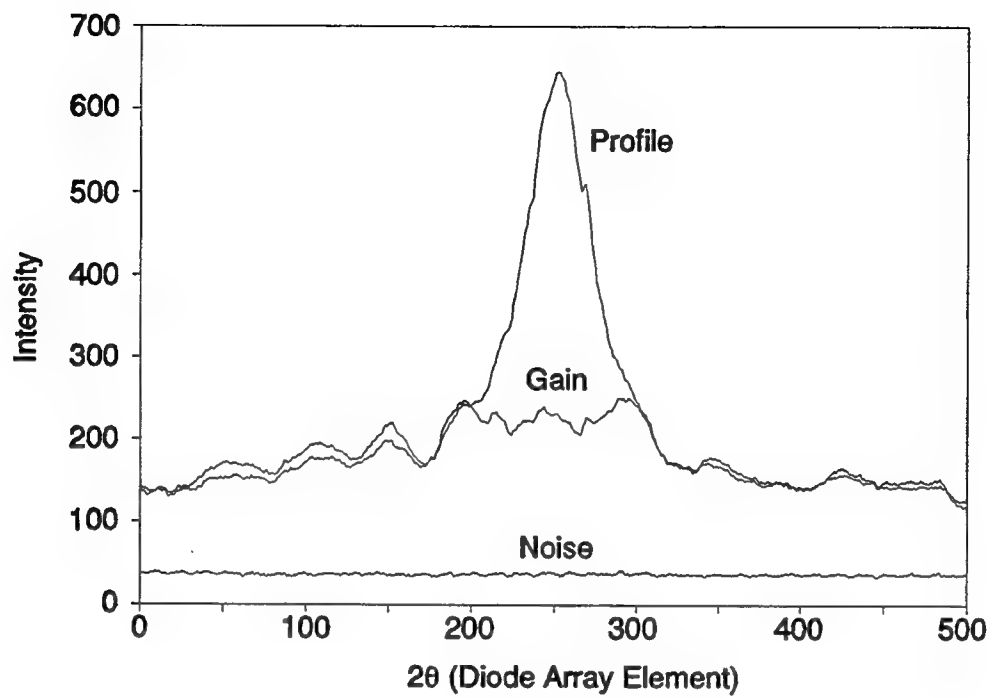
Figure 10. Left detector diffraction profiles for zero stress 400 mesh iron powder.
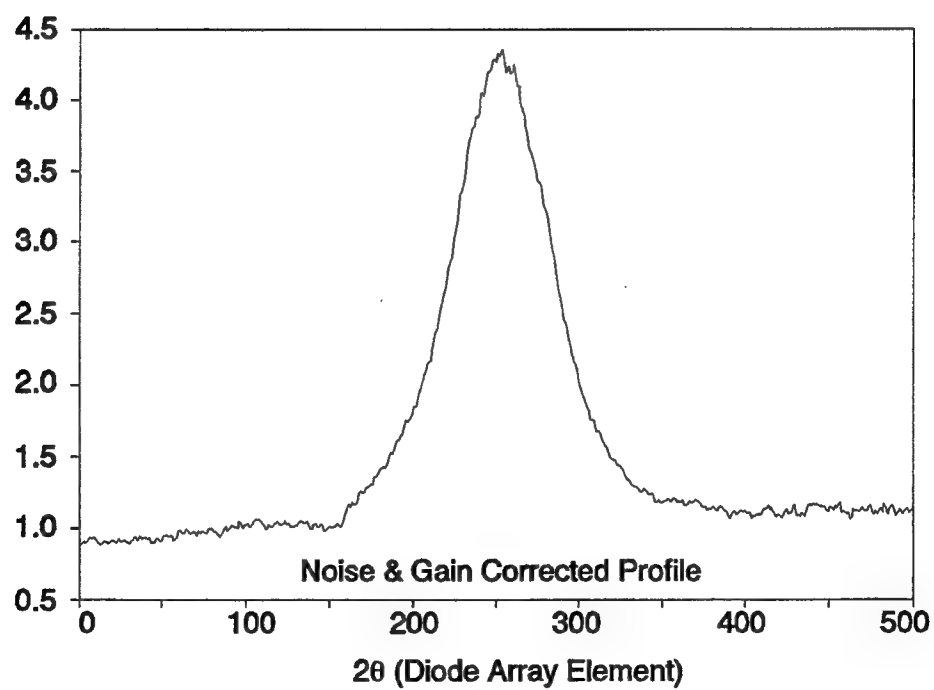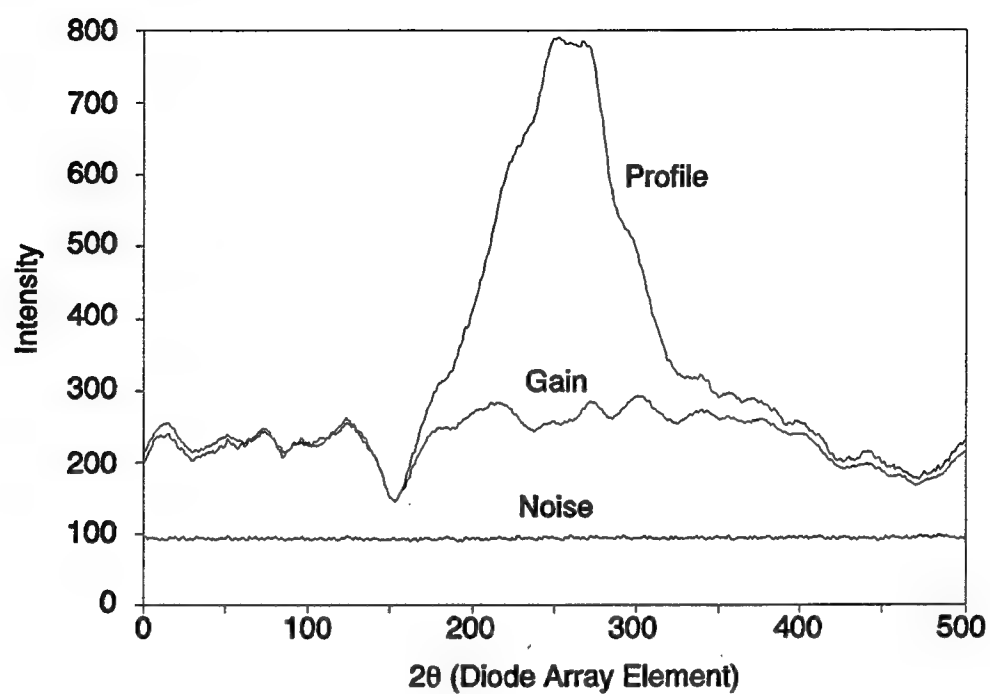
Figure 11. Right detector diffraction profiles for ferritic four-point bend specimen.
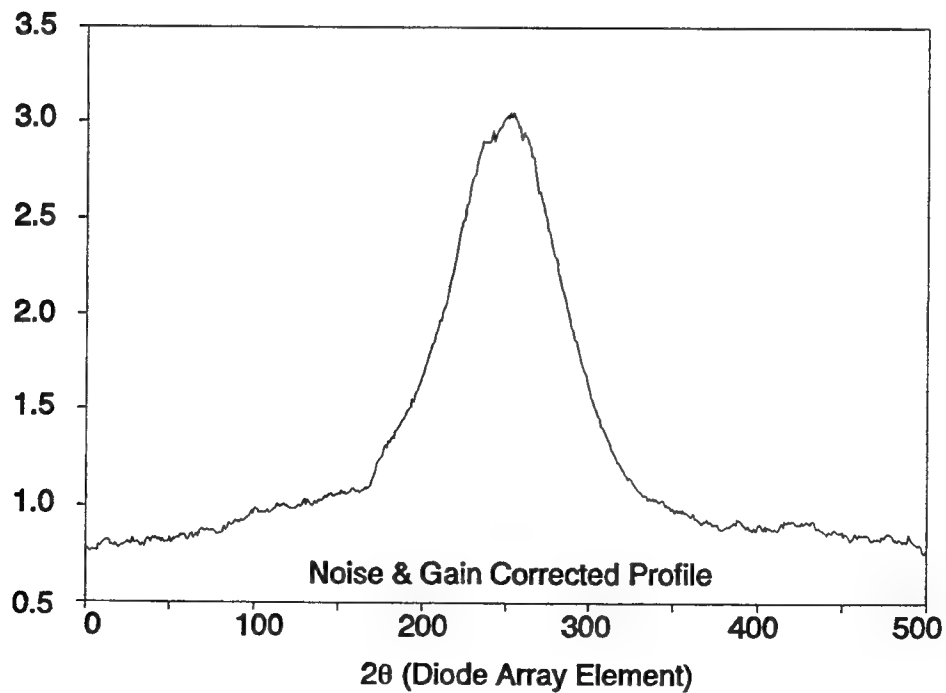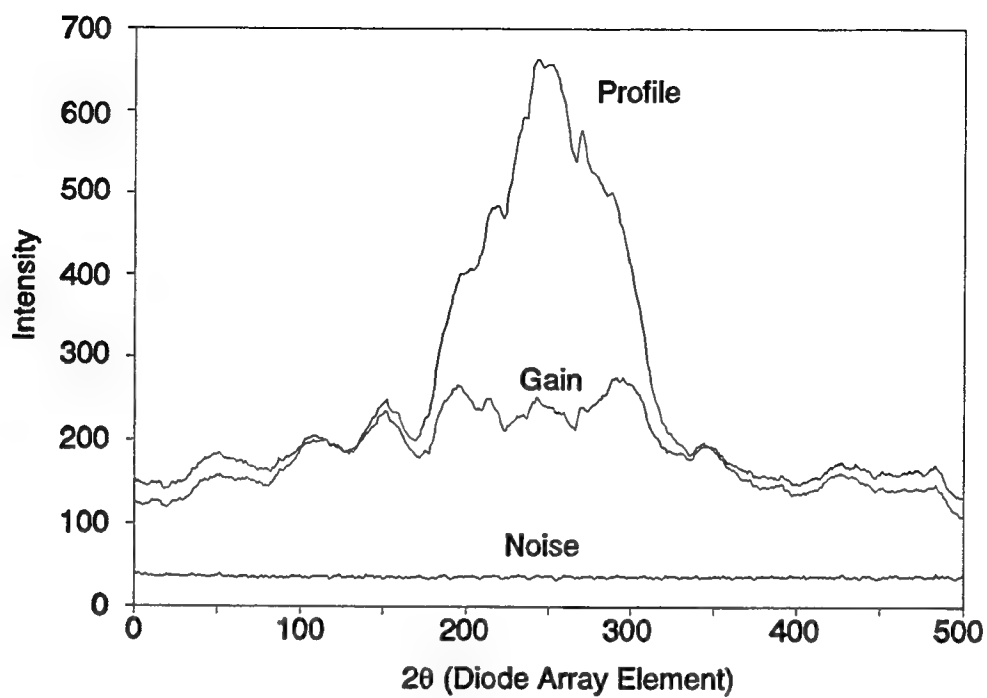
Figure 12. Left detector diffraction profiles for ferritic four-point bend specimen.
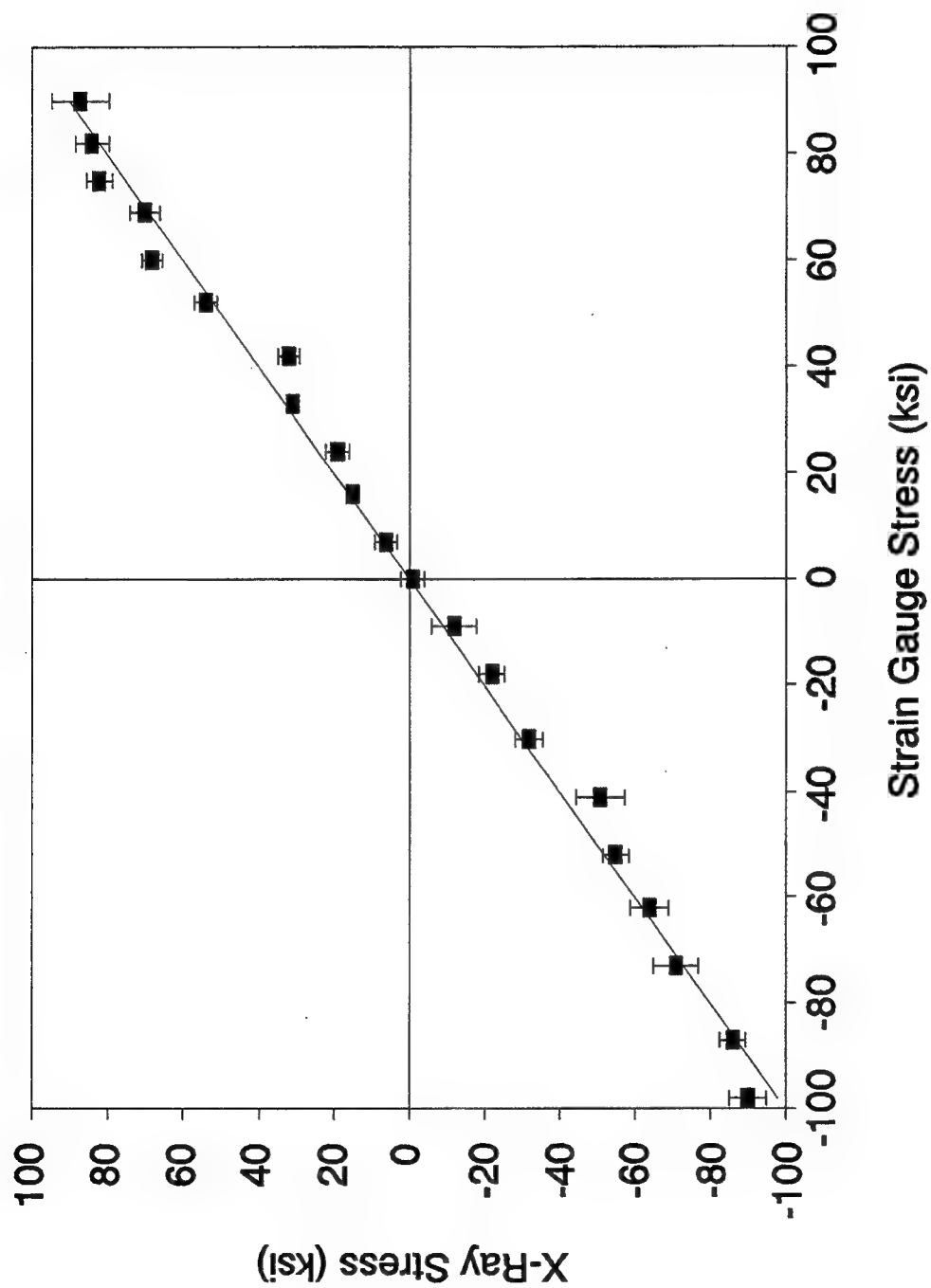
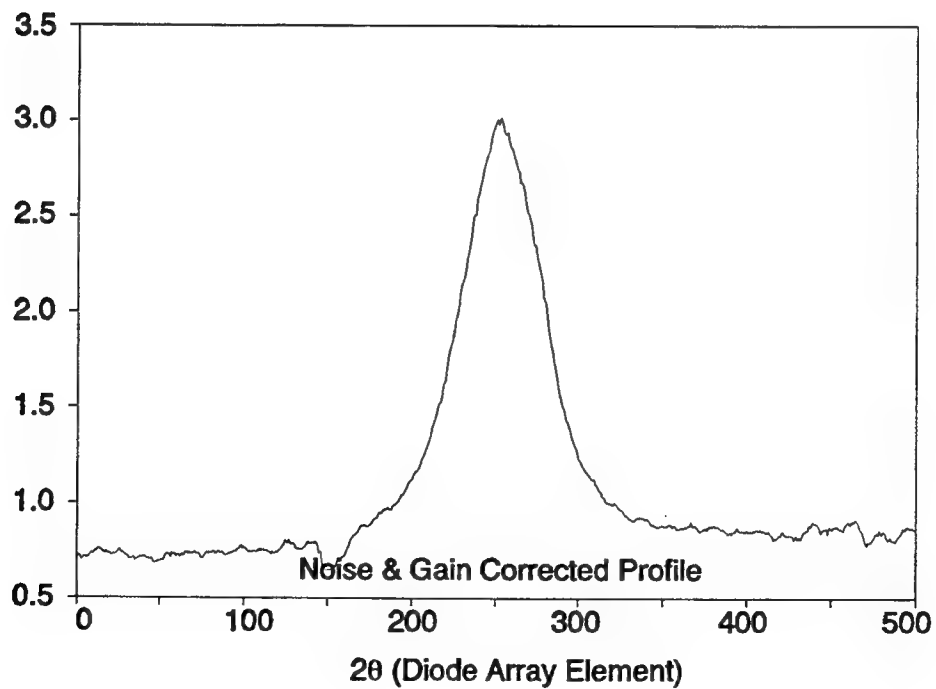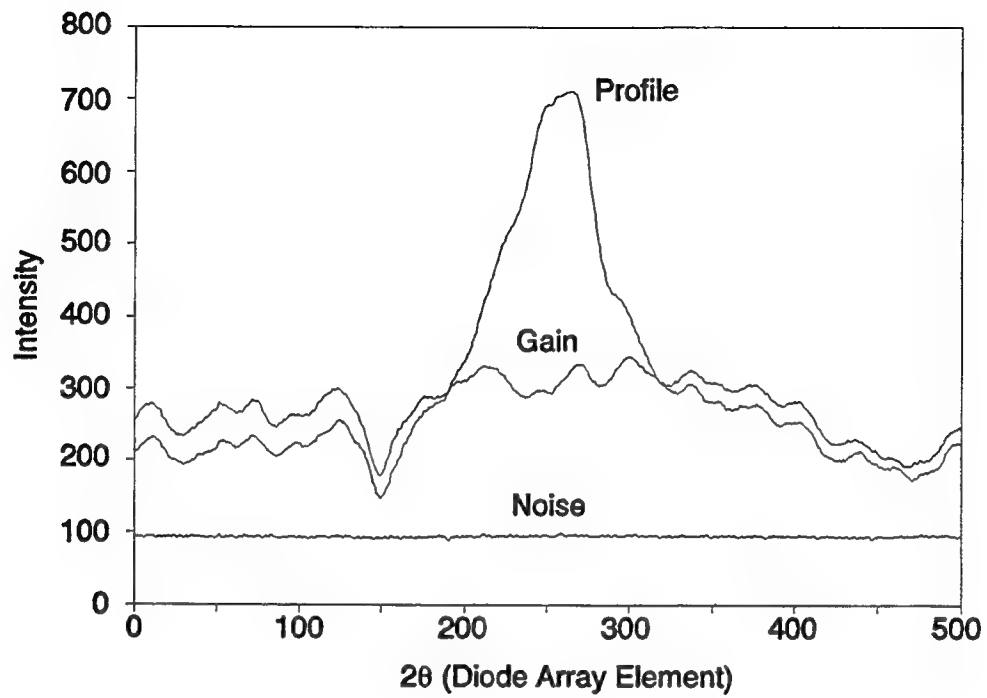Figure 13. Four-point bend verification of x-ray stress versus strain gauge stress.

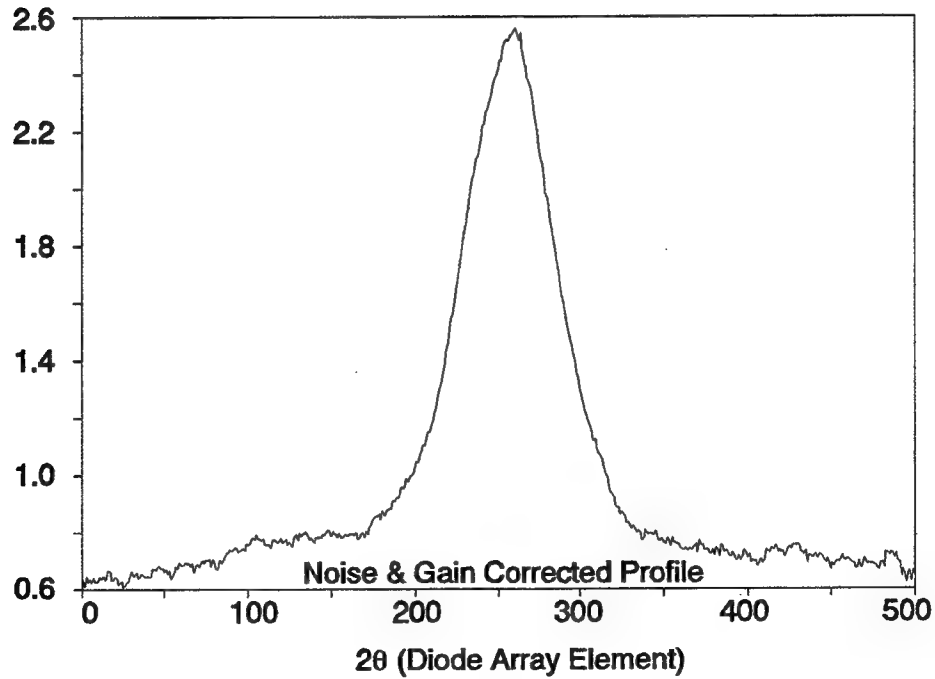Figure 14. M106 shell section inside surface axial stress right detector diffraction profiles.
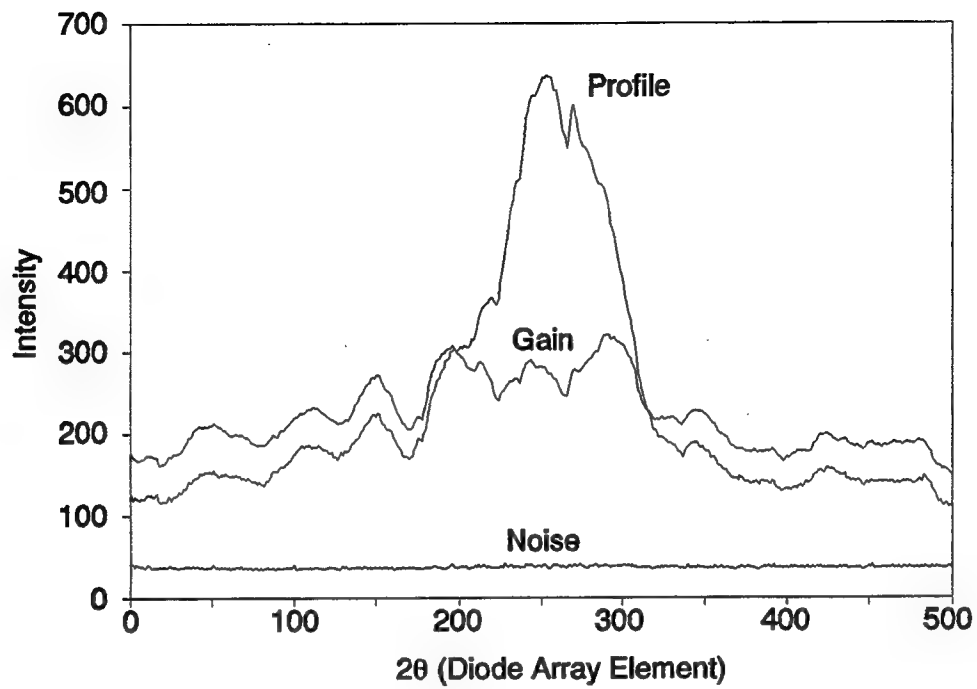
Figure 15. M106 shell section inside surface hoop stress left detector diffraction profiles.

23
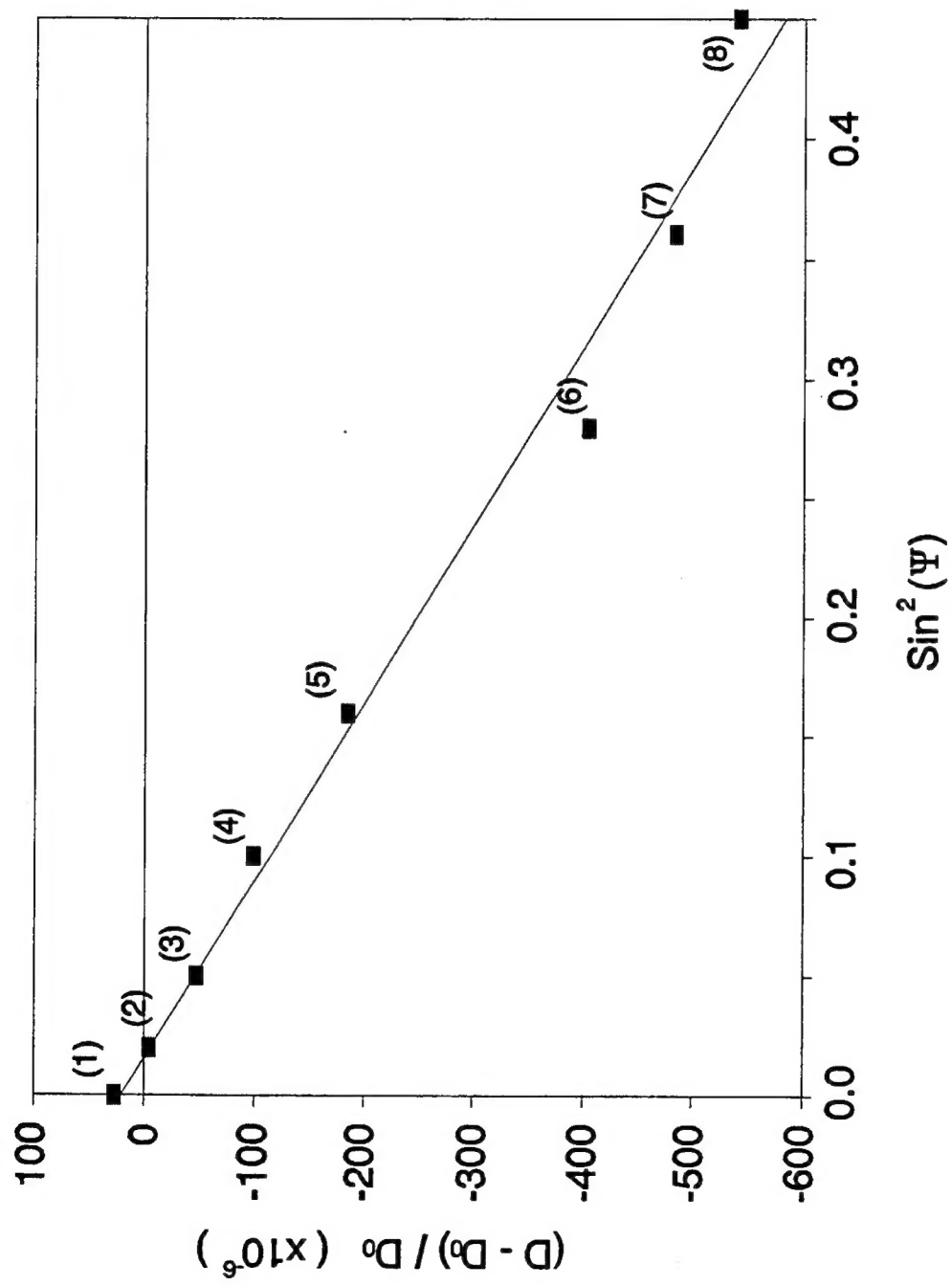
Figure 16. M106 shell section inside surface axial stress by $\sin^2(\Psi)$ technique.

24

TECHNICAL REPORT INTERNAL DISTRIBUTION LIST

	NO. OF COPIES
CHIEF, DEVELOPMENT ENGINEERING DIVISION	
ATTN: SMCAR-CCB-DA	1
-DC	1
-DI	1
-DR	1
-DS (SYSTEMS)	1
CHIEF, ENGINEERING DIVISION	
ATTN: SMCAR-CCB-S	1
-SD	1
-SE	1
CHIEF, RESEARCH DIVISION	
ATTN: SMCAR-CCB-R	2
-RA	1
-RE	1
-RM	1
-RP	1
-RT	1
TECHNICAL LIBRARY	
ATTN: SMCAR-CCB-TL	5
TECHNICAL PUBLICATIONS & EDITING SECTION	
ATTN: SMCAR-CCB-TL	3
OPERATIONS DIRECTORATE	
ATTN: SMCWV-ODP-P	1
DIRECTOR, PROCUREMENT & CONTRACTING DIRECTORATE	
ATTN: SMCWV-PP	1
DIRECTOR, PRODUCT ASSURANCE & TEST DIRECTORATE	
ATTN: SMCWV-QA	1

NOTE: PLEASE NOTIFY DIRECTOR, BENÉT LABORATORIES, ATTN: SMCAR-CCB-TL OF ADDRESS CHANGES.

TECHNICAL REPORT EXTERNAL DISTRIBUTION LIST

	NO. OF COPIES		NO. OF COPIES
ASST SEC OF THE ARMY RESEARCH AND DEVELOPMENT ATTN: DEPT FOR SCI AND TECH THE PENTAGON WASHINGTON, D.C. 20310-0103	1	COMMANDER ROCK ISLAND ARSENAL ATTN: SMCRI-ENM ROCK ISLAND, IL 61299-5000	1
ADMINISTRATOR DEFENSE TECHNICAL INFO CENTER ATTN: DTIC-FDAC CAMERON STATION ALEXANDRIA, VA 22304-6145	12	MIAC/CINDAS PURDUE UNIVERSITY P.O. BOX 2634 WEST LAFAYETTE, IN 47906	1

ASST SEC OF THE ARMY
RESEARCH AND DEVELOPMENT
ATTN: DEPT FOR SCI AND TECH   1
THE PENTAGON
WASHINGTON, D.C. 20310-0103

COMMANDER
ROCK ISLAND ARSENAL
ATTN: SMCRI-ENM   1
ROCK ISLAND, IL 61299-5000

ADMINISTRATOR
DEFENSE TECHNICAL INFO CENTER   12
ATTN: DTIC-FDAC
CAMERON STATION
ALEXANDRIA, VA 22304-6145

MIAC/CINDAS
PURDUE UNIVERSITY
P.O. BOX 2634   1
WEST LAFAYETTE, IN 47906

COMMANDER
U.S. ARMY ARDEC
ATTN: SMCAR-AEE   1
    SMCAR-AES, BLDG. 321   1
    SMCAR-AET-O, BLDG. 351N   1
    SMCAR-FSA   1
    SMCAR-FSM-E   1
    SMCAR-FSS-D, BLDG. 94   1
    SMCAR-IMI-I, (STINFO) BLDG. 59 2
PICATINNY ARSENAL, NJ 07806-5000

COMMANDER
U.S. ARMY TANK-AUTMV R&D COMMAND
ATTN: AMSTA-DDL (TECH LIBRARY)   1
WARREN, MI 48397-5000

DIRECTOR
U.S. ARMY RESEARCH LABORATORY
ATTN: AMSRL-DD-T, BLDG. 305   1
ABERDEEN PROVING GROUND, MD
  21005-5066

COMMANDER
U.S. MILITARY ACADEMY
ATTN: DEPARTMENT OF MECHANICS   1
WEST POINT, NY 10966-1792

DIRECTOR
U.S. ARMY RESEARCH LABORATORY
ATTN: AMSRL-WT-PD (DR. B. BURNS)   1
ABERDEEN PROVING GROUND, MD
  21005-5066

U.S. ARMY MISSILE COMMAND
REDSTONE SCIENTIFIC INFO CENTER   2
ATTN: DOCUMENTS SECTION, BLDG. 4484
REDSTONE ARSENAL, AL 35898-5241

DIRECTOR
U.S. MATERIEL SYSTEMS ANALYSIS ACTV
ATTN: AMXSY-MP   1
ABERDEEN PROVING GROUND, MD
  21005-5071

COMMANDER
U.S. ARMY FOREIGN SCI & TECH CENTER
ATTN: DRXST-SD   1
220 7TH STREET, N.E.
CHARLOTTESVILLE, VA 22901

COMMANDER
U.S. ARMY LABCOM
MATERIALS TECHNOLOGY LABORATORY
ATTN: SLCMT-IML (TECH LIBRARY)   2
WATERTOWN, MA 02172-0001

COMMANDER
U.S. ARMY LABCOM, ISA
ATTN: SLCIS-IM-TL   1
2800 POWER MILL ROAD
ADELPHI, MD 20783-1145

NOTE: PLEASE NOTIFY COMMANDER, ARMAMENT RESEARCH, DEVELOPMENT, AND ENGINEERING CENTER, U.S. ARMY AMCCOM, ATTN: BENÉT LABORATORIES, SMCAR-CCB-TL, WATERVLIET, NY 12189-4050 OF ADDRESS CHANGES.

	NO. OF COPIES		NO. OF COPIES
COMMANDER U.S. ARMY RESEARCH OFFICE ATTN: CHIEF, IPO P.O. BOX 12211 RESEARCH TRIANGLE PARK, NC 27709-2211	1	COMMANDER AIR FORCE ARMAMENT LABORATORY ATTN: AFATL/MN EGLIN AFB, FL 32542-5434	1
DIRECTOR U.S. NAVAL RESEARCH LABORATORY ATTN: MATERIALS SCI & TECH DIV CODE 26-27 (DOC LIBRARY) WASHINGTON, D.C. 20375	1 1	COMMANDER AIR FORCE ARMAMENT LABORATORY ATTN: AFATL/MNF EGLIN AFB, FL 32542-5434	1

NOTE: PLEASE NOTIFY COMMANDER, ARMAMENT RESEARCH, DEVELOPMENT, AND ENGINEERING CENTER, U.S. ARMY AMCCOM, ATTN: BENÉT LABORATORIES, SMCAR-CCB-TL, WATERVLIET, NY 12189-4050 OF ADDRESS CHANGES.